Effect of Test Method on Stress-Relaxation Behavior of Alloy 718

S.L. SEMIATIN, P.N. FAGIN, R.L. GOETZ, V. VENKATESH, and M.G. GLAVICIC

The stress-relaxation behavior of alloy 718 was established at 991 K (718 °C) using two contrasting test protocols. For this purpose, compression and tension samples extracted from two subscale forgings were first solution treated and cooled to room temperature. Each sample was then reheated to 991 K (718 °C), compressed or pulled isothermally to a total strain between 0.006 and 0.02, and then allowed to relax after locking either (i) the extensometer attached to the dies (compression tests) or reduced section (tension tests) or (ii) the ram itself. For the tests in compression, the stress dropped in a monotonic fashion under locked-extensometer conditions, while the locked-ram mode gave rise to a short stress drop, a broad hardening stage, and finally softening at long times. For the tension stress-relaxation tests, monotonic stress drops whose magnitudes varied for the two test modes were observed. The various behaviors were ascribed to the specific level of plastic strain imposed during the different types of tests, its quantitative effect on the level of dynamic strain aging, and thus the increment in hardening which counterbalanced stress-relaxation *per se*.

https://doi.org/10.1007/s11661-018-5092-3

I. INTRODUCTION

DURING final processing, precipitation-hardenable metallic alloys are typically solution heat treated, cooled rapidly *via* oil or water quenching, and then aged. The quenching of large components can give rise to spatially non-uniform cooling/small plastic strains which induce residual stresses. Subsequent aging may mitigate the level of residual stress concurrent with an increase in yield strength associated with precipitation *per se*. Because of the complexity of the thermomechanical phenomena during heat treatment, computer simulations can provide useful insight into the evolution of residual stress. Needless to say, such approaches require detailed descriptions of constitutive behavior, often under transient thermal and microstructural conditions.

Nickel-base superalloys are among those materials for which accurate numerical simulations of residual-stress formation would be very useful. This is because of the high cost of these materials, the need to control/limit residual-stress-induced distortion during final machining, and the possibly-beneficial effect of bulk residual stress on service properties, provided their spatial disposition and magnitude can be predicted and controlled. Despite compelling economic drivers, only a modest amount of research to simulate residual stress evolution during heat treatment of nickel-base superalloys has been reported in the open literature.[1–5] The early work of Franchet *et al.*[1] focused on residual-stress evolution during oil quenching of the powder-metallurgy (γ-γ') superalloy Astroloy. Their constitutive formulation comprised visco-plastic behavior at high temperatures and elastic–plastic behavior at low temperatures. Later work by Dye *et al.*[2] and Rist *et al.*[3] for wrought alloy 718 examined the evolution of residual stress during water/oil quenching and air cooling. These researchers used constitutive formulations consisting of a temperature-dependent yield strength or a rate-independent elastic–plastic model, respectively.

In a review article by Ma *et al.*[4] two techniques for obtaining constitutive inputs for computer simulation of residual stress were cited: on-cooling tension (or compression) tests and stress-relaxation tests. The former method, used to obtain data to simulate plastic flow during cooling following solution heat treatment, comprises preheating samples at the solution temperature, cooling at a prescribed rate to one of a series of test temperatures, holding for a short period of time for temperature equilibration, and deformation at a desired strain rate. Such tests provide flow stress as a function of strain, strain rate, and temperature for material having the metastable microstructure developed during solution treatment. The second method, the stress-relaxation test,

S.L. SEMIATIN is with the Air Force Research Laboratory, Materials and Manufacturing Directorate, AFRL/RXCM, Wright-Patterson Air Force Base, OH 45433. Contact e-mail: sheldon.semiatin@us.af.mil P.N. FAGIN is with UES, Inc., 4401 Dayton-Xenia Road, Dayton, OH 45432. R.L. GOETZ and V. VENKATESH are with Pratt & Whitney, East Hartford, CT 06108. M.G. GLAVICIC is with Rolls-Royce Corporation, Indianapolis, IN 46206.

Manuscript submitted October 17, 2018.
Article published online January 3, 2019

consists of heating and prestraining at a prescribed temperature, followed by relaxation. These experiments can provide insight into the kinetics of stress relief common during aging as well as service.[6–9]

Many of the measurements of stress-relaxation behavior for superalloys have been based on the pioneering work of Lee and Hart in the 1970s.[10] In their approach, a test sample is loaded in tension in a screw-driven test machine to a given prestrain, typically of the order of 0.01, the ram/crosshead of the testing machine is locked, and the decay of the stress as a function of time is monitored. Stress-*vs*-strain-rate results can also be determined from knowledge of the test machine stiffness and the stress-time measurements. Such a technique has been applied a number of times to characterize alloy 718, *e.g.*, References 11 and 12 in the open literature.

Several variants of the stress-relaxation test first proposed by Lee and Hart have been developed. These include tension testing in a servo-hydraulic test system in which the control signal is based on an extensometer attached to the reduced section of the tension specimen. Following the prestrain step, the extensometer position is held fixed (*i.e.*, "locked"), and the stress is allowed to relax. Because the net strain applied during relaxation is equal to zero, the instantaneous plastic strain rate is equal and opposite to the elastic strain rate; the latter is readily determined from the slope of the stress–time measurements and the Young's modulus. By this means, plots of stress *vs* plastic strain rate are readily determined.

Despite the usefulness of the stress-relaxation approach, it appears that little to no work has been performed to compare directly the effect of test variants on mechanical response. Such variants include testing in tension *vs* compression, tests in which the ram or the extensometer is locked, *etc*. The present research was undertaken to meet this need using alloy 718 as the program material. It was driven by the desire to quantify stress-relief response during long-time aging at 991 K (718 °C). For this purpose, both compression and tension stress-relaxation tests were performed in a servo-hydraulic test system for times of 6 to 8 hours. Test variables included prestrain level and relaxation mode (locked ram *vs* locked extensometer). Because of differences in sample extension/contraction associated with the two different test modes and the different gage lengths of tension and compression samples, various levels of plastic strain could thus be imposed during relaxation.

II. MATERIALS AND PROCEDURES

A. *Materials*

Alloy 718 material for stress-relaxation tests was extracted from the remnants of an axisymmetric impression-die forging (denoted as "Forging A") and a pancake forging ("Forging B").

Forging A was used previously in an investigation to establish the high-temperature Bauschinger effect.[13] From the leftover material, cylindrical compression stress-relaxation samples whose axes lay along the radial (primary-metal-flow) direction were extracted. Each sample measured 10.2-mm diameter × 15.2-mm height after cleanup *via* turning and facing in a lathe. The starting microstructure consisted of equiaxed γ grains with an average circle-equivalent diameter of 10 μm (Figure 1(a)). The grains, many of which contained annealing twins, were decorated with lenticular δ-phase particles. The Forging B remnants were large enough to extract radially-oriented compression and tension stress-relaxation samples. The compression samples had a geometry identical to those extracted from Forging A. The tension samples had an overall length of 203 mm and a reduced section with a 7.6-mm diameter and 26.7-mm length that was joined to 12.7-mm diameter shoulders *via* a 3.2-mm-radius fillet. The starting microstructure of Forging B (Figure 1(b)) was similar to that in Forging A.

B. *Stress-Relaxation Tests*

All experiments were performed in two stages comprising an initial solution-treatment step followed by prestraining and stress-relaxation testing. Both steps were conducted in custom-built fixtures utilizing induction heating (Figure 2) placed within a 250-kN servo-hydraulic test system. Solution treatment consisted of 1255 K (982 °C) for 1 hour followed by fan cooling to 755 K (482 °C) at a rate of 56 K/min (56 °C/min). Upon reaching 755 K (482 °C), each sample was then free-convection cooled to room temperature.

For the compression stress-relaxation tests, an extensometer was placed on the dies following the solution treatment. The probes were located as close as possible to (but not on) the sample due to space limitations (Figure 2(a)). The test sample was then reheated to 991 K (718 °C), soaked 10 min, prestrained under extensometer control to a total (elastic + plastic) prestrain between 0.006 and 0.02 at a strain rate of 0.01 s^{-1}, and allowed to relax for 6 to 8 hours. During the relaxation, either the extensometer position was kept fixed (*i.e.*, the extensometer was "locked") or the ram position was locked. This was accomplished by controlling the actuator using the extensometer or ram, respectively. The corresponding tension tests were performed similarly except that the extensometer probes were placed between the turns of the induction coil onto the reduced section of the specimen (Figure 2(b)). It should be noted that a reproducibly-uniform temperature was maintained along the sample and dies in compression (beyond the location at which the extensometer probes were placed) and along the reduced section and shoulders in tension by adjustment of the induction coils and use of flux concentrators. Quantitative consideration of the temperature field of the outer, cooler portions of the load train was unnecessary due to the use of the extensometer data for all trials. Despite the presence of the temperature gradient, however, it should be borne in mind that the majority of the relaxation in locked-ram tests was due to deflection associated with the

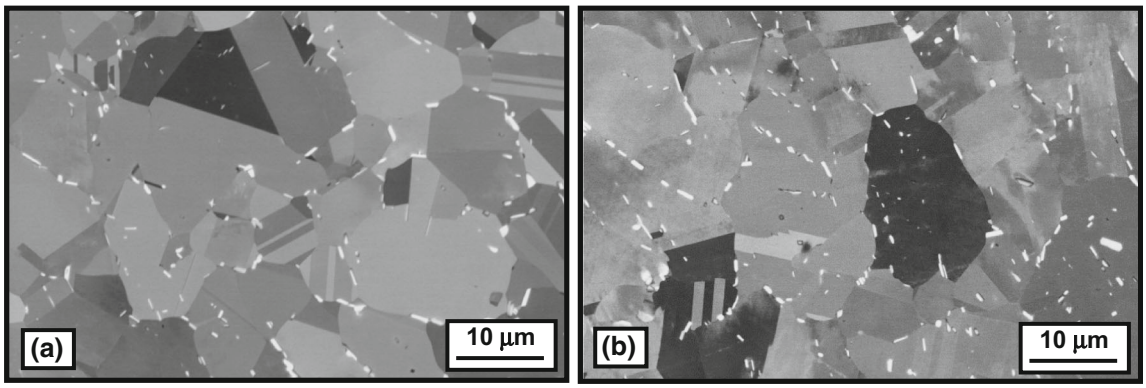

Fig. 1—Microstructure of alloy 718 in the as-received condition: (*a*) Forging A and (*b*) Forging B.

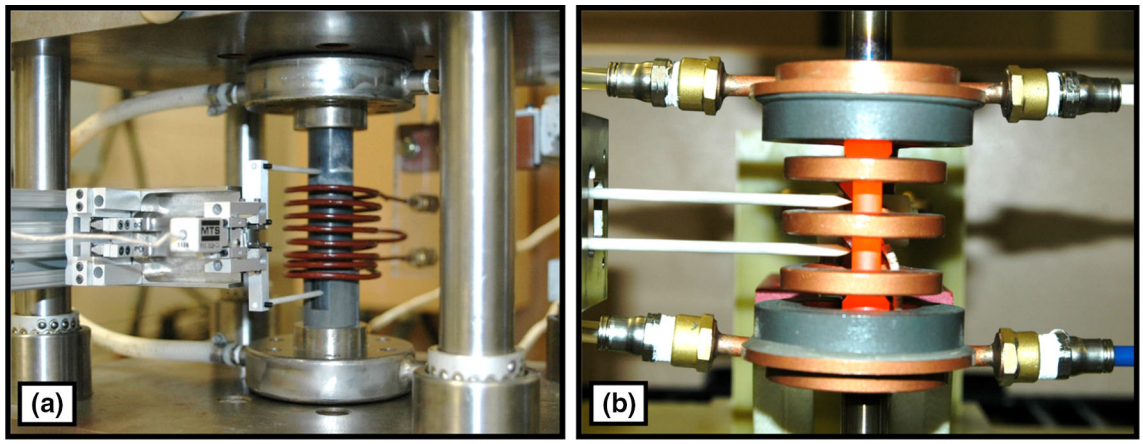

Fig. 2—Photographs of tooling used for (*a*) compression and (*b*) tension stress-relaxation tests. For the compression tests, each of the extensometer probes was placed on a die at an axial position lying ~27 mm from the corresponding die-workpiece interface location.

load-cell construction and not the cooler portions of the tooling.

A true stress–true strain curve for the prestrain portion of each experiment was obtained from the load-extension data. The principal outputs of the relaxation portion of each experiment comprised plots of load/stress *vs* time and total (elastic + plastic) extension/strain *vs* time. For the compression experiments performed under locked-extensometer conditions, the dies underwent a small, but finite, elastic unloading during relaxation. The instantaneous *tension* displacement associated with the die unloading was estimated from a *die-stack* compliance curve measured between the extensometer probes at 755 K (482 °C) for the range of loads of interest here. (In previous work, it was found that the compliance of the ceramic tooling is very small and varies negligibly for the range of temperatures of interest in the present work.) From such data, the associated sample *compressive* deflection and hence the *total compressive sample strain vs* time during relaxation were determined. Data reduction for the compression test for which the ram (rather than the extensometer) was locked involved an identical analysis of stress-*vs*-time and sample-strain-*vs*-time plots, the latter deduced from (1) the extensometer measurements, (2) the die-stack compliance, and (3) stress-*vs*-time data. For the corresponding tension tests, such corrections were not necessary inasmuch as the total extension was measured directly on the reduced section. The evolution of the plastic strain during relaxation as a function of time for both the compression and tension types of tests was determined by subtracting the instantaneous elastic strain (equal to the change in stress during relaxation divided by Young's modulus) from the total strain.

The sample *plastic strain rate* at a number of levels of stress was also calculated by subtracting the elastic strain rate (determined from the slope of the stress-*vs*-time plot and Young's modulus) from the total strain rate (from the slope of the total strain-*vs*-time curve) at corresponding times/stresses. Subsequently, the stress-plastic strain rate results were plotted in log–log form to obtain estimates of the strain-rate sensitivity of the flow stress.

For all of the results below, compressive stresses and strains are reported as positive quantities as are the tension stresses and strains.

C. *Metallography*

Selected compression samples were examined to establish microstructure evolution before and during stress relaxation. Metallographic preparation comprised

grinding with SiC papers down to 800 grit, rough polishing with diamond, final polishing with colloidal silica, and etching in a solution of 33 pct nitric acid, 33 pct glacial acetic acid, 33 pct deionized water, and 1 pct hydrofluoric acid. The area fraction of γ'' was determined *via* point counting on secondary-electron (SE) micrographs taken at magnifications of 100 and 150 kX using a Zeiss Gemini scanning electron microscope (SEM). Imaging was performed using an accelerating voltage of 0.5 kV, working distance between 3 and 4 mm, and aperture size of 20 μm. At least two typical images (superimposed with ~3000 point-count grid intersections) were used for each test condition. The number of precipitates per unit area was also determined manually for each heat-treatment condition. From the precipitate area fraction and number-density results, the average two-dimensional (2D) circle-equivalent diameter (CED) was determined; the uncertainty in this quantity was estimated to be less than 10 pct of the values reported below.

III. RESULTS

The principal results of this investigation comprised true-stress–true strain curves, stress-relaxation (stress-*vs*-time) curves, strain-*vs*-time plots, log–log plots of stress *vs* plastic strain rate, and microstructure observations.

A. *Flow Curves and Relaxation Behavior: Forging A*

The mechanical behavior of Forging A (which was tested in compression only) is summarized in Figures 3, 4, and 5. Each of the true stress–true strain curves (Figure 3 for samples prestrained either ~0.006 or 0.01) exhibited a nominally elastic loading to a yield strength (proportional limit) of ~475 MPa, modest strain hardening to the end of the prestrain stage (at which the maximum stress was achieved), and then a drop in stress

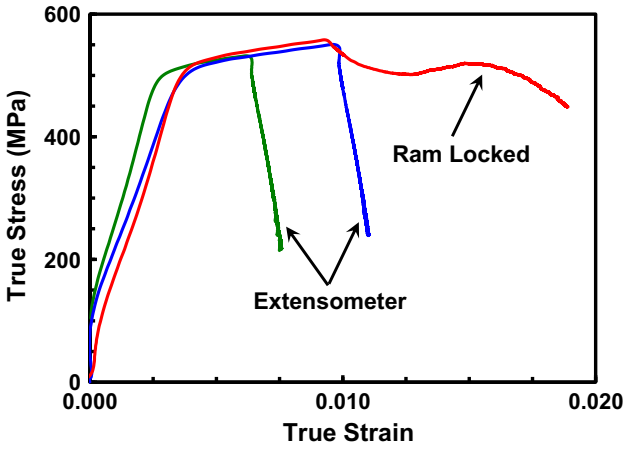

Fig. 3—True stress–true strain curves for Forging A compression samples prestrained either 0.006 (green curve) or 0.01 (blue, red curves) and then relaxed under locked-extensometer control (green, blue curves) or locked-ram control (red curve) (Color figure online).

when the extensometer or ram was locked during the relaxation stage. For the two cases in Figure 3 for which the extensometer was locked, the stress dropped monotonically. A noticeably-different behavior was observed for the 0.01-prestrain case for which the ram was locked. In this instance, the stress dropped initially, then increased, and finally decreased. The flow behaviors were examined in more detail *via* plots of stress *vs* time for the entire test (Figure 4(a)) or the initial portion of each test (Figure 4(b)). For the two experiments in which the extensometer was locked, the stress-*vs*-time curves showed the typical exponential decay for the entire relaxation interval. The degree of the drop in stress was similar for these two cases for which the prestrain was either 0.006 or 0.01. After long time (~30,000 seconds), the sample prestrained 0.006 showed a flow stress which was approximately 25 MPa *lower* than the sample prestrained 0.01. This difference was comparable to the difference in flow stress at the end of the prestraining stage for the two samples (Figure 3). However, close examination of the stress-time behaviors at shorter times (Figure 4(b)) revealed that the stress difference during relaxation was initially very small and grew over time. The observed behavior may be due to experimental scatter. Alternatively, the trend may suggest that the larger prestrain may have accelerated dynamic precipitation onto/solute diffusion to dislocations, albeit to a relatively small degree. In addition, the stress-*vs*-time results for the two locked-extensometer tests in Figure 4 exhibited serrations comprising a series of small sequential load drops. Such serrations are typically associated with the unlocking of dislocations from solutes/solute atmospheres.[14,15] In particular, Hale *et al.*[15] have demonstrated that chromium is the solute responsible for this behavior at high temperatures such as that used in the present work.

In contrast to the stress-*vs*-time behavior for the locked-extensometer experiments, the case for which the ram was locked exhibited an early drop in stress (until a time of ~500 seconds), subsequent hardening to a stress plateau (at ~6250 seconds), and then softening for the balance of the test (red curves in Figure 4). In contrast to the locked-extensometer observations, the stress-*vs*-time behavior for the locked-ram test in Figure 4 exhibited only very minor waviness and no marked serrations.

As suggested by the relaxation portion of the flow curves in Figure 3, the strain-*vs*-time behaviors differed noticeably for the two types of experiments (Figure 5). A plot of total (elastic + plastic) strain as a function of time (Figure 5(a)) revealed the difference in a semi-quantitative fashion. For the locked-extensometer case, the change in strain with time was associated with the small elastic unloading of the portion of each die between the extensometer probe and the corresponding die-workpiece interface. The total sample strain imposed during relaxation was thus relatively small, *i.e.*, ~0.001 to 0.0015. By contrast, the total strain imposed during relaxation for the locked-ram experiment was substantially larger, *i.e.*, ~0.009. This larger strain can be ascribed to the large elastic unloading/lengthening of the entire load train/load-cell structural members, which in turn produced a large compressive deflection/strain in

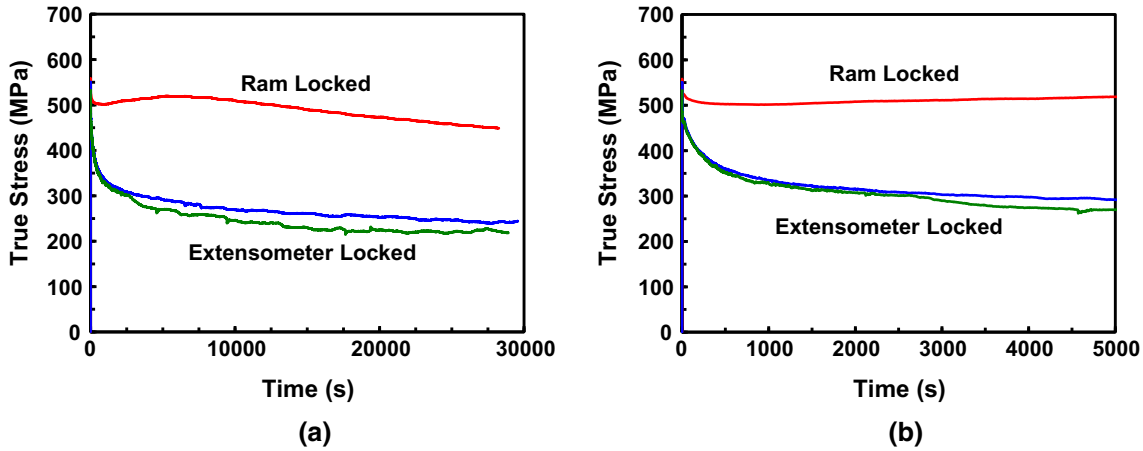

Fig. 4—True stress-*vs*-time behaviors for Forging A compression samples prestrained either 0.006 (green curves) or 0.01 (blue, red curves) and then relaxed under locked-extensometer control (green, blue curves) or locked-ram control (red curve). The data are plotted in terms of (*a*) the overall long-time observations and (*b*) short-time observations (Color figure online).

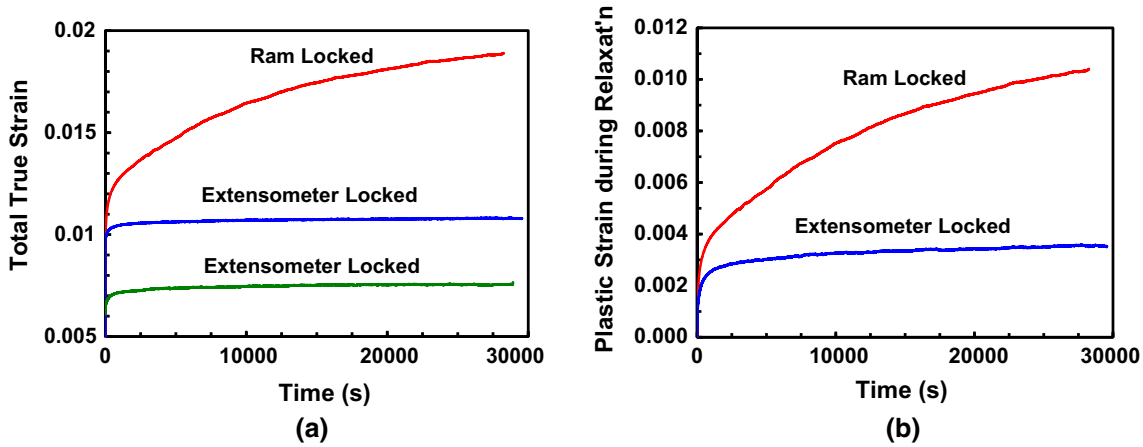

Fig. 5—True strain-*vs*-time behaviors for Forging A compression samples prestrained either 0.006 (green curves) or 0.01 (blue, red curves) and then relaxed under locked-extensometer control (green, blue curves) or locked-ram control (red curve). The data are plotted in terms of (*a*) total strain developed during the entire test or (*b*) plastic strain developed during the relaxation stage (Color figure online).

the sample. Furthermore, it was noted that the relaxation strain was ~0.005 at the time at which the peak flow stress had been achieved (~6250 seconds) for the locked-ram sample.

The different behaviors exhibited in Figure 5(a) were further elucidated in a quantitative fashion by focusing on the *plastic strain* developed during relaxation as a function of time (Figure 5(b)). The plastic strain developed for the locked-extensometer case involving a prestrain of 0.01 was 0.003. Most of this plastic strain had been imposed by a time of ~5000 seconds. On the other hand, the plastic strain developed during the corresponding locked-ram test was 0.0105, approximately one-half of which had been imposed by 5000 seconds.

B. *Flow Curves and Relaxation Behavior: Forging B*

Compression and tension experiments using samples extracted from Forging B shed further light on the range of behaviors that were obtained during stress-relaxation testing with the current load frame and tooling.

Behavior in *compression* for Forging B was analogous to that found for Forging A. For example, the flow response during prestraining (Figure 6(a)) was similar. The only major difference was a slightly-higher yield stress (proportional limit) for Forging B (*i.e.*, 530-540 MPa) and peak stresses at the end of the prestrain interval (*e.g.*, ~500 MPa for Forging A and ~550 MPa after a prestrain of 0.01). Such differences may be ascribed to slight differences in the crystallographic texture developed during closed- *vs* open-die forging, different levels of strain/stored work imparted during forging which may not have been totally eliminated during sub-delta-solvus solution treatment, *etc*. Second, the flow curves during the relaxation period were similar. Locked-extensometer trials showed a monotonic drop in stress, and locked-ram cases exhibited an initial drop, a transient hardening stage, and then another drop.

The relaxation trends noted in the compression flow curves for Forging B were mirrored in the stress-*vs*-time plots (Figure 6(b)). The locked-extensometer results

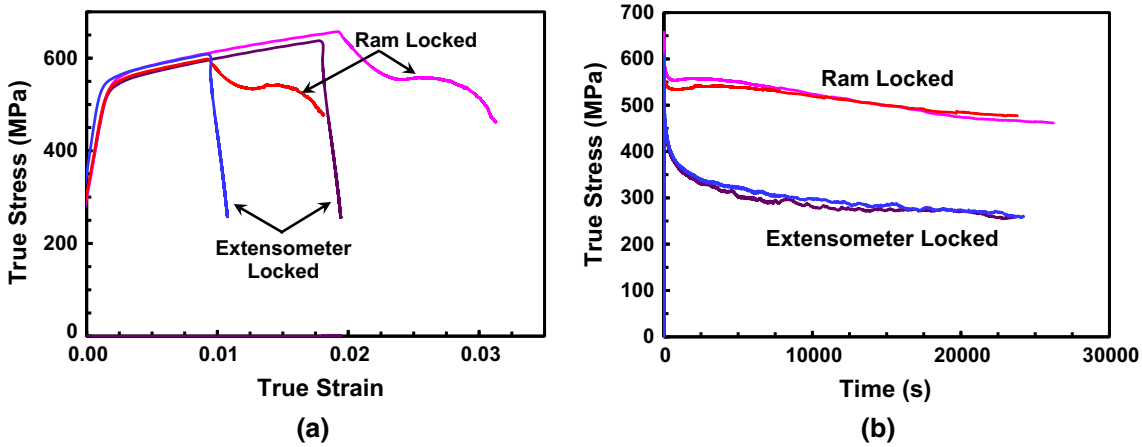

Fig. 6—Mechanical test results for Forging B compression samples: (*a*) True stress–true strain curves and (*b*) stress-*vs*-time behaviors for samples prestrained either 0.01 (blue, red curves) or 0.02 (purple, pink curves) and then relaxed under locked-extensometer control (blue, purple curves) or locked-ram control (red, pink curves) (Color figure online).

showed the classical exponential decay of stress with time, much as was found during the corresponding data for Forging A (Figure 4). Although the flow stress just before relaxation was ~50 MPa higher for the prestrain of 0.02 in comparison with that for the 0.01 prestrain, the stress-relaxation curves for the locked-extensometer trials merged rapidly after a time of ~35 s, an observation perhaps due to experimental scatter. The locked-extensometer stress-*vs*-time curves for Forging B also revealed evidence of serrated-yielding behavior, although the form of the discontinuities differed from those for Forging A (Figure 4(a)). The stress-*vs*-time results for the locked-ram cases for Forging B (Figure 6(b)) were very similar to those for Forging A (Figure 5). The only measurable difference was a slightly lower degree of hardening during the early transient for Forging B; this observation was almost the same irrespective of prestrain.

The temporal dependences of the total strain and plastic strain during the relaxation stage for Forging B compression tests (Figure 7) were also very similar to those found for Forging A (Figure 5), at least qualitatively. The key difference lay in the values of plastic strain imposed during the relaxation stage (Figure 7(b)). For the locked-extensometer cases, this strain was ~0.004 at the end of relaxation, or a value slightly greater than that noted for the corresponding Forging A cases (*i.e.*, ~0.003). For the locked-ram trials on Forging B, the plastic strains at the end of relaxation were either ~0.01 (prestrain = 0.01) or 0.0135 (prestrain = 0.02). At least a portion of the difference in plastic strain for these two cases can be ascribed to the higher flow stress/load achieved during a prestrain of 0.02 and thus greater deflection of the load cell/load train during relaxation compared to that for the prestrain of 0.01.

The behavior in *tension* for Forging B samples showed some similarities and some differences relative to the results found in compression for both forgings. By and large, the flow curves (Figure 8(a)) were similar to those measured in compression for both forgings (Figures 3 and 6(a)) with the quantitative behavior somewhat closer to that for Forging A. Again, differences in texture and stored work in the specific locations from which test samples were extracted can be used to rationalize this finding. More importantly, the stress-*vs*-time data for the Forging B tension tests (Figure 8(b)) contrasted with those from the compressions tests. Specifically, both the locked-extensometer and locked-ram results exhibited a broad exponential decrease of stress with time as well as various degrees of serrated flow. However, the magnitude of the exponential decrease depended on the test protocol. Not unexpectedly, the stress drop during relaxation was noticeably greater for the locked-extensometer trials. However, the minimum flow stress achieved by the end of these trials (~350 MPa) was ~100 MPa greater than that achieved in the corresponding compression stress-relaxation tests for the two forgings (Figures 4(a) and 6(b)). The source of this difference warrants further investigation.

The difference in the stress-relaxation behavior for the locked-ram trials performed in tension (Figure 8(b)) *vs* those in compression (Figures 4(a) and 6(b)) can be rationalized on the basis of the magnitudes of the corresponding levels of strain imposed during relaxation. First, the total strains in the locked-ram tension tests (Figure 9(a)) were smaller in comparison to those in the compression tests. This difference can be ascribed to the smaller cross-sectional area and longer gage length of the tension specimens compared to those for the compression specimens. The smaller cross-sectional area led to lower loads during prestraining and thus smaller load train deflections which promoted subsequent relaxation. Second, the longer gage length of the tension specimens produced smaller imposed strains for a given load-train deflection. The effect of such differences on deformation response was further quantified in the plots of plastic strain *vs* time for the tension tests (Figure 9(b)). These results revealed an approximately two-fold reduction in plastic strain developed during relaxation in tension under locked-ram conditions, *i.e.*, ~0.005 in tension *vs* ~0.01 in compression.

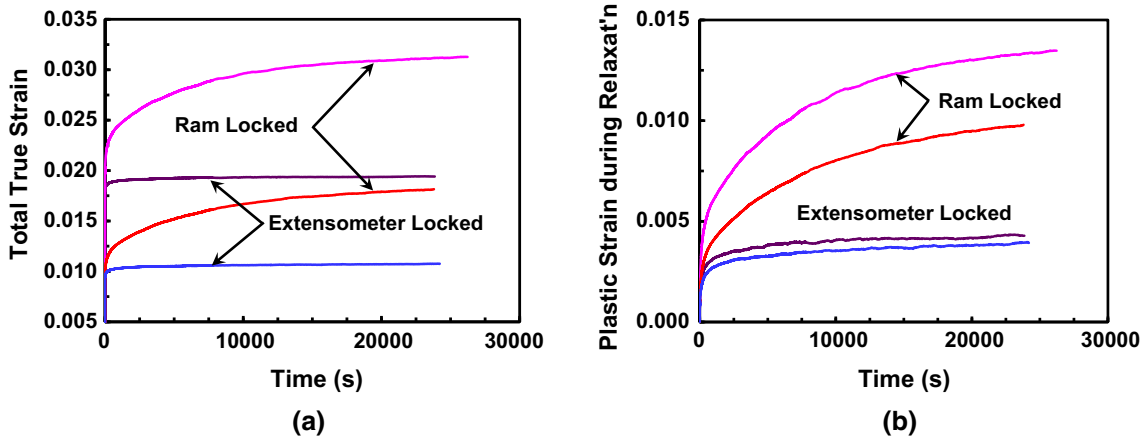

Fig. 7—True strain-*vs*-time behaviors for Forging B compression samples prestrained either 0.01 (blue, red curves) or 0.02 (purple, pink curves) and then relaxed under locked-extensometer control (blue, purple curves) or locked-ram control (red, pink curves). The data are plotted in terms of (*a*) total strain developed during the entire test or (*b*) plastic strain developed during the relaxation stage (Color figure online).

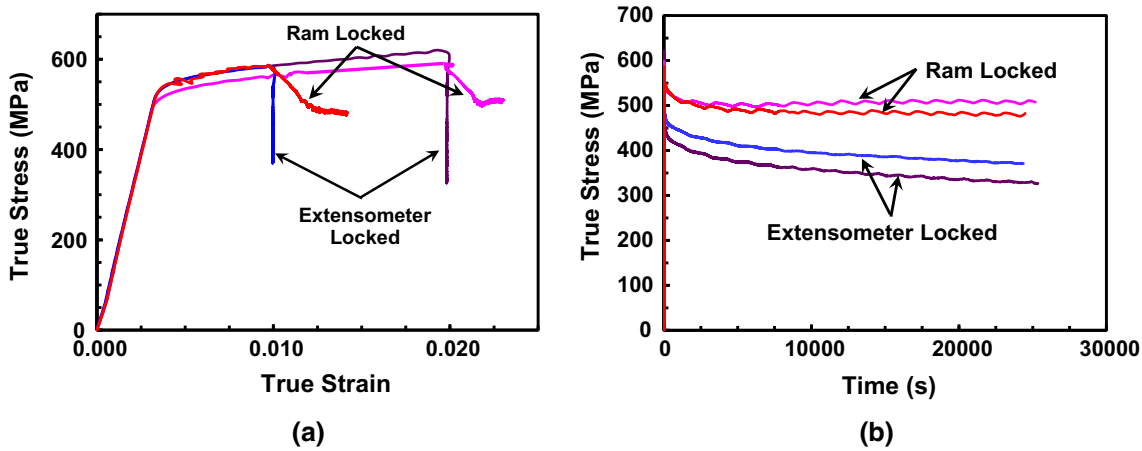

Fig. 8—Mechanical test results for Forging B tension samples: (*a*) True stress–true strain curves and (*b*) stress-*vs*-time behaviors for samples prestrained either 0.01 (blue, red curves) or 0.02 (purple, pink curves) and then relaxed under locked-extensometer control (blue, purple curves) or locked-ram control (red, pink curves) (Color figure online).

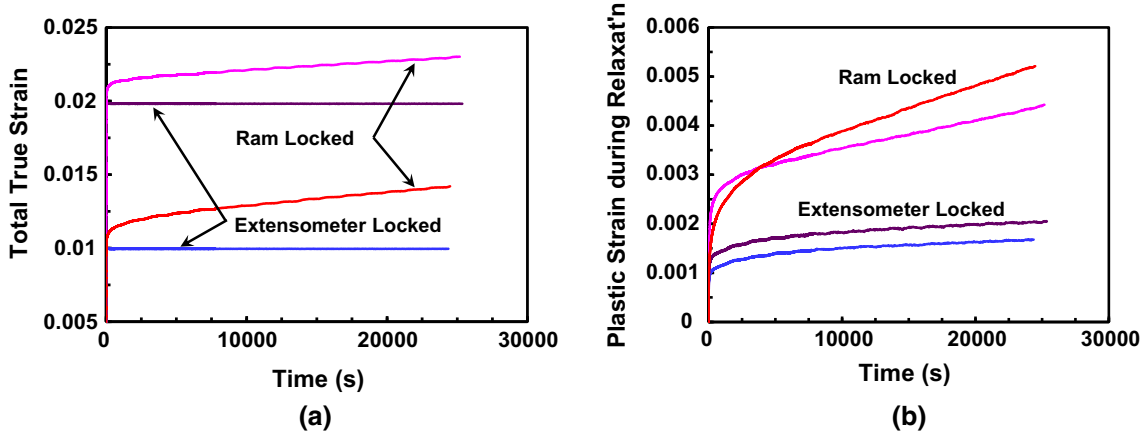

Fig. 9—True strain-*vs*-time behaviors for Forging B tension samples prestrained either 0.01 (blue, red curves) or 0.02 (purple, pink curves) and then relaxed under locked-extensometer control (blue, purple curves) or locked-ram control (red, pink curves). The data are plotted in terms of (*a*) total strain developed during the entire test or (*b*) plastic strain developed during the relaxation stage (Color figure online).

The total strain plots showed no change with time during relaxation for the tension tests performed under locked-extensometer conditions (Figure 9(a)). This observation was expected inasmuch as the extensometer was attached to the reduced section for the tension tests and thus confirmed the ability of the servo-hydraulic actuator to move in response to the zero-extension/deflection command signal for such cases. On the other hand, the plastic strains developed during locked-extensometer tension-stress-relaxation tests (Figure 9(b)), *i.e.*, ~0.0015, were approximately one half those developed during the corresponding tests in compression, *i.e.*, ~0.003 (Figures 5(b) and 7(b)).

C. *Microstructure Observations*

High-resolution SEM BSE micrographs did not indicate a likely source for the difference in stress-relaxation behavior for locked-extensometer and locked-ram conditions. At low magnification, the microstructures comprised equiaxed γ grains with a small volume fraction (< 5 pct) of remnant δ particles which had not been dissolved during the initial subsolvus solution treatment at 1255 K (982 °C). Figure 10 shows typical high-magnification micrographs of the structures developed during compression experiments for Forging A. For example, a micrograph of a solution-heat-treated sample that had been reheated to 991 K (718 °C), prestrained 0.01, and then forced-convection cooled exhibited no evidence of γ'' (or γ') precipitation (Figure 10(a)). The apparent absence of precipitation in this sample differs from the experimental observations of Chaturvedi *et al.*[16] and simulation predictions of Zhang *et al.*[17] and may have been a result of the lack of high-enough resolution in the SEM-imaging method used in the present work. By contrast, samples that had been prestrained and then subjected to stress relaxation under either locked-extensometer or locked-ram conditions all showed an extensive array of fine precipitates (Figures 10(b) through (d)). Based on isothermal-transformation data in the literature (Figure 11),[18,19] these precipitates were likely γ''. Moreover, the morphology of the precipitates in 718 tend to be either disk-shaped (γ'') or spheroidal (γ'). Such differences could not be detected in the present micrographs and would likely require transmission electron microscopy, whose use was beyond the scope of the present work. Quantitative metallography (Table I) revealed that the precipitate volume fractions were in the range between 7 and 13 pct with average circle-equivalent diameters between 11 and 15 nm. To a first order, the locked-ram condition appeared to give rise to a slightly-smaller volume fraction of finer precipitates compared those generated under locked-extensometer conditions.

IV. DISCUSSION

The present measurements revealed a distinct effect of testing protocol (*i.e.*, locked-extensometer *vs* locked-ram)

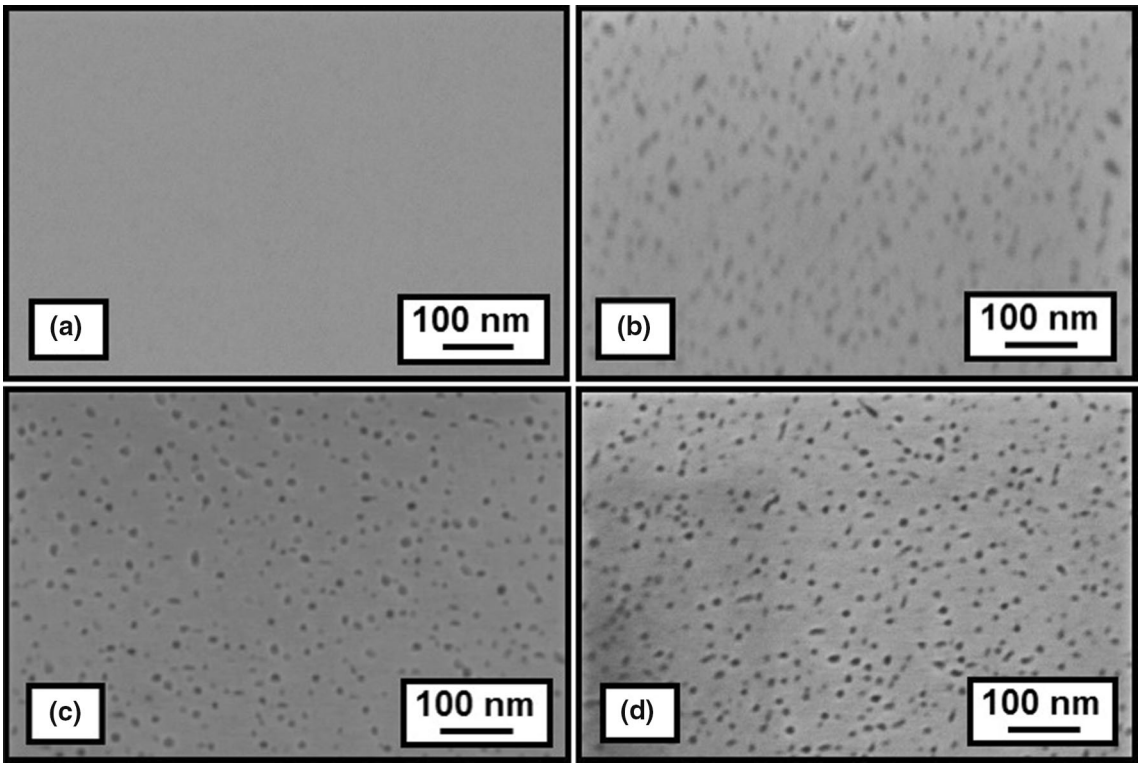

Fig. 10—High-resolution, high-magnification SEM SE images of precipitates developed in Forging A compression samples which had been (*a*) prestrained 0.01 and then cooled or prestrained (*b*) 0.006 or (*c*, *d*) 0.01 and then relaxed under (b, c) locked-extensometer or (d) locked-ram conditions.

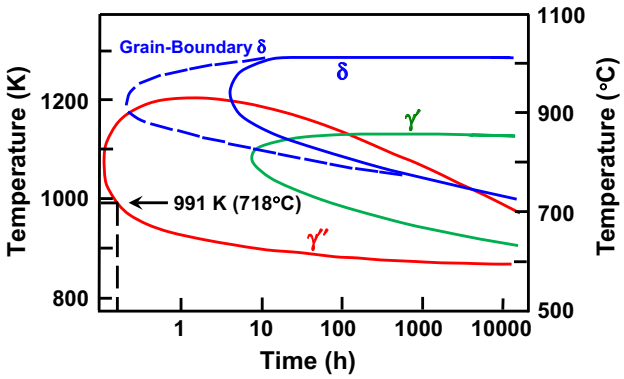

Fig. 11—Isothermal-transformation diagram for alloy 718.[18,19]

Table I. Precipitate Measurements for Forging A Compression Samples

SR Mode	Prestrain	Area Fraction	2D Dia (nm)
—	0.01	0	—
Ext Locked	0.006	0.13	14.6
Ext Locked	0.01	0.11	11.8
Ram Locked	0.01	0.07	10.9

on the stress-relaxation behavior of alloy 718 at a temperature [991 K (718 °C)] in the range often used for aging/stabilization heat treatment following solution treatment. From a broad perspective, several, likely-interacting, factors can be hypothesized to play a role in controlling the mechanical response during stress relaxation. These include plastic strain *per se*, precipitate formation, and solute diffusion. Plastic strain can produce strain hardening due to the generation of dislocations while the dislocations formed during prestraining or concurrently with stress relaxation can serve as nucleation sites for precipitates as well as have their motion retarded by precipitates or solutes. Because of the complexity of this problem, only some initial hypotheses can therefore be put forward at this time.

A. *Strain-Hardening Effect on Stress Relaxation*

An estimate of the possible effect of differences in plastic strain and thus strain hardening on stress-relaxation response can be determined from the flow curves generated during the prestraining stage (*e.g.*, Figure 3 for compression stress-relaxation tests on Forging A). These curves suggest that the application during relaxation of an additional plastic strain of the order of 0.01 would lead to strain hardening of the order of 50 MPa. The differences in stress between locked-ram and locked-extensometer tests in compression are of the order of 200 to 250 MPa, however. Thus, strain hardening *per se* cannot explain the difference in the two behaviors.

B. *Precipitation Effect on Stress Relaxation*

The possible effect of precipitation on the observations was interpreted in terms of prior measurements of the isothermal-transformation (IT) behavior of alloy 718 (Figure 11).[18,19] At 991 K (718 °C), the static precipitation of γ'' appears to commence at 610 seconds. (This time varies among different measurements in the literature of IT behavior for alloy 718, but it is likely a good order-of-magnitude estimate.) The value of ~600 seconds is comparable to the times at which the locked-ram stress-*vs*-time curves in compression tests reached local minima and began experiencing a hardening transient (Figure 4 for Forging A, Figure 6(b) for Forging B). Thus, it may be surmised that precipitation may indeed have had a role in the stress-relaxation observations for this mode of testing. In this regard, prior work on high-strength, low-alloy (HSLA) steels[20] suggests that either prestrain or concurrent straining can noticeably *reduce* the time for the onset of precipitation, contradictory to the present hypothesis. The difference between the present 718 and prior HSLA observations may lie with the much larger plastic strains and higher plastic strain rates utilized in the earlier steel work. Despite such reasoning for the present locked-ram compression stress-relaxation tests, the hypothesis regarding an effect of concurrent precipitation on relaxation cannot explain the *absence* of a hardening transient in the compression stress-relaxation tests under locked-extensometer conditions, let alone all of the tension stress-relaxation experiments.

Additional doubt on precipitation as a source of the difference in relaxation behavior during locked-ram *vs* locked-extensometer relaxation in compression arises upon inspection of the results in Table I. Although these precipitate measurements represent only the end point in long-time stress-relaxation experiments, they do show little difference in precipitate size and volume fraction for the two types of test methods, especially for the comparison comprising an identical prestrian of 0.01. A similar conclusion can be drawn perhaps from the work of Calvi *et al.*[21] who performed locked-extensometer stress-relaxation trials for 718, albeit only for temperatures higher than that employed here, *i.e.*, ≥ 1073 K (800 °C). In particular, for samples prestrained 0.005 and relaxed at 1073 K (800 °C), these former researchers noted an initial hardening transient during the time interval between ~10 and 60 seconds. However, they found *no* precipitates in a sample water quenched after 60 seconds. The occurrence of precipitation *per se* may also be thought to influence the analysis of stress-relaxation behavior through its effect on the elastic modulus and volume changes associated with the phase change. With regard to the former effect, it has been found that Young's modulus (E) increases ~5 pct relative to that of single-phase γ due to the precipitation of γ''.[22] Data reduction using such a higher value of E has indicated almost negligible changes in plots of the temporal variation in plastic strain for both locked-extensometer and locked-ram experiments. The effect of precipitation on volume/length changes is discussed in Section IV–D below.

C. *Solute Diffusion/Locking Effect on Relaxation*

The third, and final, possibility hypothesized as the source of the effect of test mode on stress-relaxation behavior relates to solute diffusion and concomitant locking of dislocations. With respect to this possibility,

Hale *et al.*[15] quantified dynamic-strain-aging (DSA) response for a fine-grain sheet of alloy 718 which had been solution treated at 1200 K (927 °C) prior to tension tests at temperatures between 300 K (27 °C) and 1000 K (727 °C) and strain rates between 10^{-4} and 10^{-1} s^{-1}. In the higher-temperature portion of this range, serrated flow was observed at 923 K (650 °C), but not higher temperatures, irrespective of strain rate; similar trends were also found by Max *et al.*[23] Moreover, the high-temperature DSA behavior was shown to be associated with substitutional solutes such as chromium.

In the present work, the test temperature of 991 K (718 °C) was thus in the region for which DSA was not noted by Hale *et al.* However, the temperature/strain rate boundary separating the presence and absence of DSA may depend on the precise temperature at which solution treatment is performed prior to lower-temperature mechanical testing as well as the type of test machine. In the present work, solution treatment was done ~50 K (50 °C) above that used in the former research; moreover, a servo-hydraulic machine was used in the present work, whereas Hale *et al.* used a screw-driven machine. Thus, it may be surmised that the sporadic observations of what appears to be serrated flow during relaxation in the present work may indicate conditions close to a boundary between the occurrence and absence of DSA and thus the occurrence of solute diffusion *and* locking of dislocations. Such processes could be complementary in that higher dislocation contents generated by larger amounts of plastic flow during relaxation would promote both enhanced (pipe) diffusion and hardening when the migration of these dislocations is retarded by the solutes.

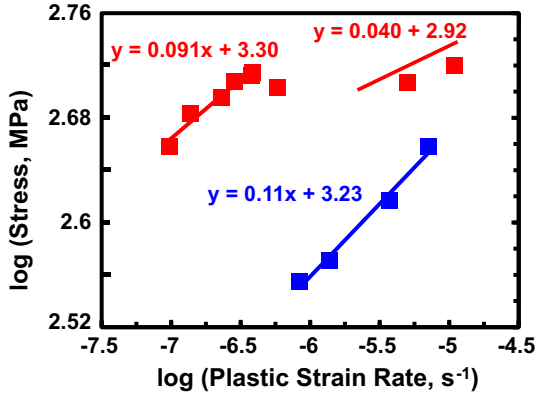

Fig. 12—Log-log plots of stress *vs* plastic strain rate from compression stress-relaxation tests for Forging A involving a prestrain of 0.01 under a locked-extensometer condition (blue data points/trend line) or locked-ram condition (red data points/trend lines) (Color figure online).

The possibility that the present tests involved deformation close to the boundary between the presence and absence of DSA was further supported by low values of the strain-rate sensitivity of the flow stress (m) derived from the stress-relaxation data; typical results are shown in Figures 12 and 13 for Forgings A and B, respectively. In most cases, the m values were of the order of 0.05 or less. The principal exception to this trend was the short-time behavior for locked-ram tests during which the flow stress increased as the plastic strain rate decreased (strain rate $\approx 10^{-6}$ s^{-1}, red data in Figure 12); *i.e.*, m was negative. Flow curve measurements in Reference 13 for the same lot of material as that used in the present research also suggested that the present deformation conditions lay close to a transition region. Specifically, the previous work revealed noticeably serrated flow (and negligible rate sensitivity) at 922 K (649 °C) and strain rates of 0.003 and 0.0001 s^{-1}. It was also seen at 1033 K (760 °C), but only for the higher of these two strain rates.

D. *Phenomenological Correlation of Observations*

The apparent correlation of the degree of stress relaxation and imposed plastic strain is quantified in Figure 14. Here, the fractional stress drop parameter for each experiment in the present work was defined operationally as $(\sigma_p - \sigma_{20,000})/\sigma_p$ in which σ_p denotes the flow stress at the end of the prestrain stage and

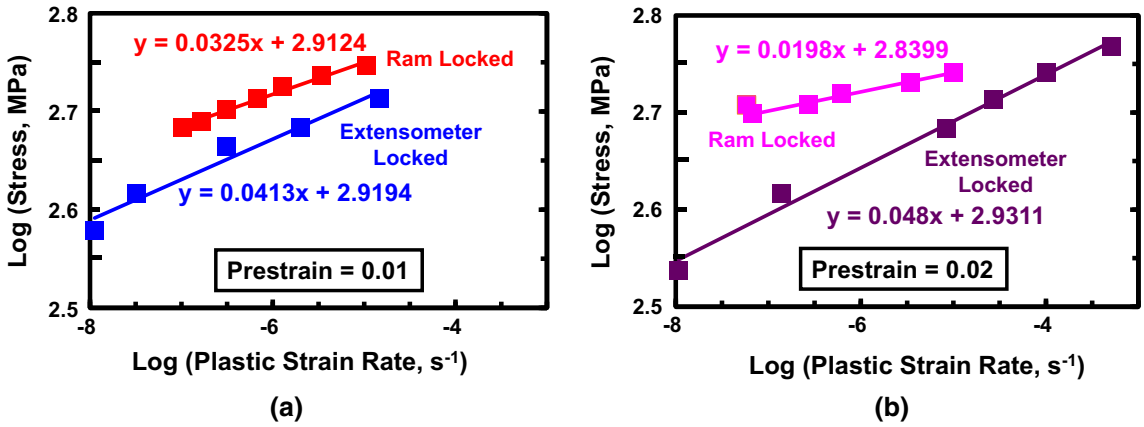

Fig. 13—Log-log plots of stress *vs* plastic strain rate from tension stress-relaxation tests for Forging B involving a prestrain of (*a*) 0.01 or (*b*) 0.02 under a locked-extensometer condition (blue, purple data points/trend lines) or locked-ram condition (red, pink data points/trend lines) (Color figure online).

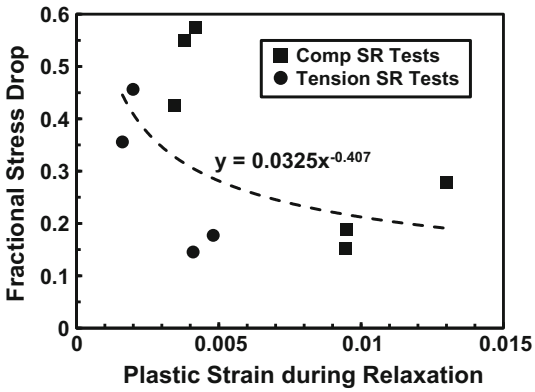

Fig. 14—Plot of the stress-drop parameter as a function of plastic strain imposed during relaxation from the end of prestraining to a time of 20,000 s.

$\sigma_{20,000}$ is the stress after 20,000 seconds of relaxation. Although there is a moderate amount of scatter in the results in Figure 14, a broad trend corresponding to an approximately inverse-square-root dependence of stress drop on plastic strain can be noted. From a qualitative standpoint, this dependence might be rationalized on the basis of the classical Taylor relation between stress and the square root of dislocation density/strain. Future work to further quantify this relation is warranted. Very recent measurements of the volume change during aging at 993 K (720 °C) of solution annealed samples of alloy 718[24] have revealed a linear shrinkage strain of the order of 0.0005 over an 8-hour period. Consideration of such a phase-change strain for the results in Figure 14 would move the compression points relatively-slightly to the left and the tension points slightly to the right, but would not noticeably affect the overall trend shown in the plot.

V. SUMMARY AND CONCLUSIONS

The stress-relaxation behavior for solution-heat-treated alloy 718 at a typical aging temperature [991 K (718 °C)] exhibited distinctly-different behaviors depending on whether the extensometer or ram was held fixed (“locked”) during the test. The following conclusions were drawn from this work:

1. When the extensometer is locked, the stress decreases monotonically with time. On the other hand, for testing under a locked-ram condition, the stress decreases initially, exhibits a hardening transient, and then decreases again at long times.
2. The difference in locked-extensometer *vs* locked-ram behaviors can be ascribed to differences in the level of plastic strain imposed during relaxation. For the tooling used in the present work, the plastic strains imparted during compression stress relaxation were of the order of 0.003 for locked-extensometer conditions and 0.012 for locked-ram conditions. For longer-gage-length tension samples, the corresponding plastic strains were approximately one-half those developed in compression.
3. The stress-relaxation behavior under a given test mode exhibits a limited dependence on prestrain in the range between 0.006 and 0.02.
4. The micro-mechanism that most likely controls the test-mode dependence on stress relaxation appears to be solute diffusion/dislocation locking.
5. The present work suggests the absence of a unique relation between the magnitude of stress relaxation and time at least at 991 K (718 °C). Hence, simulations of stress-relaxation behavior during aging following solution treatment or in service should consider the influence of concurrent deformation.

ACKNOWLEDGMENTS

Portions of this research were conducted in support of the AFRL Materials and Manufacturing Directorate’s Foundational Engineering Problem (FEP) on bulk residual-stress development in nickel-base superalloys performed under the auspices of the Metals Affordability Initiative, Contract No. FA8650-13-2-5201. The support and encouragement of the FEP Program Managers (B. Song, T.J. Turner, and M.J. Caton) are gratefully acknowledged. The authors also thank Drs. C.S. Lee, G.A. Sargent, J. Cormier, and J.M. Cabrera for insightful technical discussions regarding stress-relaxation testing/concurrent phase transformations and N.C. Levkulich for performing the metallography. One of the authors (R.L. Goetz) was with Rolls-Royce Corporation, Indianapolis, IN during the early portion of the work.

REFERENCES

1. J.M. Franchet, F. Devy, P.E. Mosser, Y. Honnorat, and A. Benallal: in *Superalloys 1992*, S.D. Antolovich, R.W. Stusrud, R.A. MacKay, D.L. Anton, T. Khan, R.D. Kissinger, and D.L. Klarstrom, eds. TMS, Warrendale, PA, 1992, pp. 73–82.
2. D. Dye, K.T. Conlon, and R.C. Reed: *Metall. Mater. Trans. A*, 2004, vol. 35A, pp. 1703–13.
3. M.A. Rist, S. Tin, B.A. Roder, J.A. James, and M.R. Daymond: *Metall. Mater. Trans. A*, 2006, vol. 37A, pp. 459–67.
4. K. Ma, R.L. Goetz, and S.K. Srivatsa: in *ASM Handbook, Vol. 22B: Metals Process Simulation*, D.U. Furrer and S.L. Semiatin, eds., ASM International, Materials Park, OH, 2010, pp. 386–408.
5. R.A. Wallis and P.R. Bhowal: in *Superalloys 1988*, S. Reichman, D.N. Duhl, G. Maurer, S. Antolovich, and C. Lund, eds. TMS, Warrendale, PA, 1988, pp. 525–34.
6. M. Khadhraoui, W. Cao, L. Castex, and J.Y. Guedou: *Mater. Sci. Technol.*, 1997, vol. 13, pp. 360–67.
7. T.P. Gabb, J. Telesman, P.T. Kantzos, P.J. Bonacuse, R.L. Barrie, and D.J. Hornbach: *TMS Ltrs*, 2004, vol. 5, pp. 115–16.
8. D. Cai, P. Nie, J. Shan, W. Liu, Y. Gao, and M. Yao: *J. Mater. Eng. Perform.*, 2006, vol. 15, pp. 614–17.
9. P.E. Aba-Perea, T. Pirling, and M. Preuss: *Mater. Des.*, 2016, vol. 110, pp. 925–31.
10. D. Lee and E.W. Hart: *Metall. Trans.*, 1971, vol. 2, pp. 1245–48.
11. O. Bapokutty, Z. Sajuri, and S. Syarif: *J. Appl. Sci.*, 2012, vol. 12, pp. 870–75.
12. S. Rahimi, M. King, and C. Dumont: *Mater. Sci. Eng., A*, 2017, vol. 708, pp. 563–73.
13. S.L. Semiatin, P.N. Fagin, B. Streich, R.L. Goetz, and V. Venkatesh: in *Proc. 9th Inter. Symp. On Superalloy 718 & Derivatives: Energy, Aerospace, and Industrial Applications*, E. Ott, et al., eds., Springer International, New York, 2018, pp. 957–75.

14. P. Rodriguez: *Bull. Mater. Sci.*, 1984, vol. 6, pp. 653–63.
15. C.L. Hale, W.S. Rollings, and M.L. Weaver: *Mater. Sci. Eng. A*, 2001, vol. 300, pp. 153–64.
16. M.C. Chaturvedi and Y.-F. Han: *Metal Sci*, 1983, vol. 17, pp. 145–49.
17. F. Zhang, W. Cao, C. Zhang, S. Chen, J. Zhu, and D. Lv: *in Proceedings, 9th International Symposium on Superalloy 718 & Derivatives: Energy, Aerospace, and Industrial Applications,* E. Ott, ed., TMS, Pittsburgh, 2018, pp. 147–61.
18. A. Thomas, M. El-Wahabi, J.M. Cabrera, and J.M. Prado: *J. Mater. Proc. Technol.*, 2006, vol. 177, pp. 469–72.
19. C. Slama and G. Cizeron: *J. Phys. III*, 1997, vol. 7 (3), pp. 665–88.
20. I. Weiss and J.J. Jonas: *Metall. Trans. A*, 1979, vol. 10A, pp. 831–40.
21. J. Calvi, S. Shu, and J.M. Cabrera: *Mater. Sci. Forum*, 2012, vols. 706–709, pp. 2393–99.
22. J. Cormier: Institut P', ISAE-ENSMA, Chasseneuil-Futuroscope, France, Private Communication, 2018.
23. B. Max, B. Viguier, E. Andrieu, and J.M. Cloue: *Metall. Mater. Trans. A*, 2014, vol. 45A, pp. 5431–41.
24. H. Qin, Z. Bi, D. Li, R. Zhang, T.L. Lee, G. Feng, H. Dong, J. Du, and J. Zhang: *Mater. Sci. Eng. A*, 2019, in press.